Editors' Suggestion | Featured in Physics

Subfemtosecond Tracing of Molecular Dynamics during Strong-Field Interaction

Václav Hanus,[1,*] Sarayoo Kangaparambil,[1] Seyedreza Larimian,[1] Martin Dorner-Kirchner,[1] Xinhua Xie (谢新华),[1,2] Markus S. Schöffler,[3] Gerhard G. Paulus,[4] Andrius Baltuška,[1] André Staudte,[5,†] and Markus Kitzler-Zeiler[1,‡]

[1]*Photonics Institute, Technische Universität Wien, 1040 Vienna, Austria, EU*
[2]*SwissFEL, Paul Scherrer Institute, 5232 Villigen PSI, Switzerland*
[3]*Institut für Kernphysik, Goethe-Universität Frankfurt, 60438 Frankfurt, Germany, EU*
[4]*Institute for Optics and Quantum Electronics, Friedrich-Schiller-Universität Jena, 07743 Jena, Germany, EU*
[5]*Joint Laboratory for Attosecond Science of the National Research Council and the University of Ottawa, Ottawa, Ontario K1A 0R6, Canada*

(Received 12 July 2019; published 23 December 2019)

We introduce and experimentally demonstrate a method where the two intrinsic timescales of a molecule, the slow nuclear motion and the fast electronic motion, are simultaneously measured in a photoelectron photoion coincidence experiment. In our experiment, elliptically polarized, 750 nm, 4.5 fs laser pulses were focused to an intensity of 9×10^{14} W/cm^2 onto H_2. Using coincidence imaging, we directly observe the nuclear wave packet evolving on the $1s\sigma_g$ state of H_2^+ during its first round-trip with attosecond temporal and picometer spatial resolution. The demonstrated method should enable insight into the first few femtoseconds of the vibronic dynamics of ionization-induced unimolecular reactions of larger molecules.

DOI: 10.1103/PhysRevLett.123.263201

Molecular fragmentation and isomerization processes are of fundamental importance in nature. These nuclear rearrangement processes are initiated and ultimately determined by electronic dynamics that can be influenced by precisely timed distortions of the electronic structure with the electric field of strong, ultrashort laser pulses [1–4]. For example, fine variations of the delay between successive ionization events can determine the number of moieties produced during fragmentation of polyatomic molecules [5]. To reveal the dynamics underlying these processes, it is necessary to apply probing techniques that are sensitive to both the fast electronic dynamics that may take place on attosecond timescales and the slower nuclear motion taking place on the femtosecond timescale. While even the fastest vibrational wave packet in H_2^+ has been probed successfully shortly *after* its creation using a pump-probe scheme with near-single-cycle pulses [6,7], it is, however, a major obstacle to trace the molecular dynamics *during* the first few femtoseconds of the interaction of a molecule with a strong laser pulse.

In this Letter, we introduce and experimentally demonstrate a method capable of tracing simultaneously electronic and vibrational wave packet dynamics in a fragmenting molecule on subfemtosecond times. The method combines the subcycle sensitivity inherent to angular streaking that has been applied to studying ionization dynamics in atoms [8–12] and molecules [13–16], with the high structural sensitivity of Coulomb explosion imaging [17–21] to resolve vibrational motion. Our work is inspired by earlier attempts [22] of constructing such a method, which has been called *the molecular clock*.

We investigate the applicability of this concept by tracing the nuclear and electronic dynamics in H_2^+ triggered by the emission of an electron over several femtoseconds. Upon ionization of H_2^+ various scenarios can take place [23]. The simplest one is that a vibrational wave packet is created on the $1s\sigma_g$ energy level following the Franck-Condon (FC) principle [24], see Fig. 1(a). Even for this simplest of all cases it has been shown that the very fast nuclear motion taking place during the ionization event can lead to deviations from the population distribution of vibrational states predicted by the FC principle [25]. In another scenario, shake-up excitations can lead to the population of vibrational states not only on the $1s\sigma_g$ but also on the $2p\sigma_u$ level [26]. In recent photoelectron holography measurements evidence for subcycle population transfer to $2p\sigma_u$ was found [27]. As the vibrational dynamics proceeds after ionization in the presence of the strong laser field, three- or five-photon resonant excitations can lead to partial population transfer between the $1s\sigma_g$ and $2p\sigma_u$ levels [1,2]. We show that we can achieve temporal and spatial resolutions of a few tens of attoseconds and about 1 pm—sufficient to disentangle these different scenarios.

To obtain attosecond temporal resolution we employ angular streaking [8,9] illustrated in Fig. 1(b). Angular streaking exploits the direct mapping of electron momentum to the instantaneous laser electric field at the time of ionization. In elliptically polarized light the electric field

 © 2019 American Physical Society

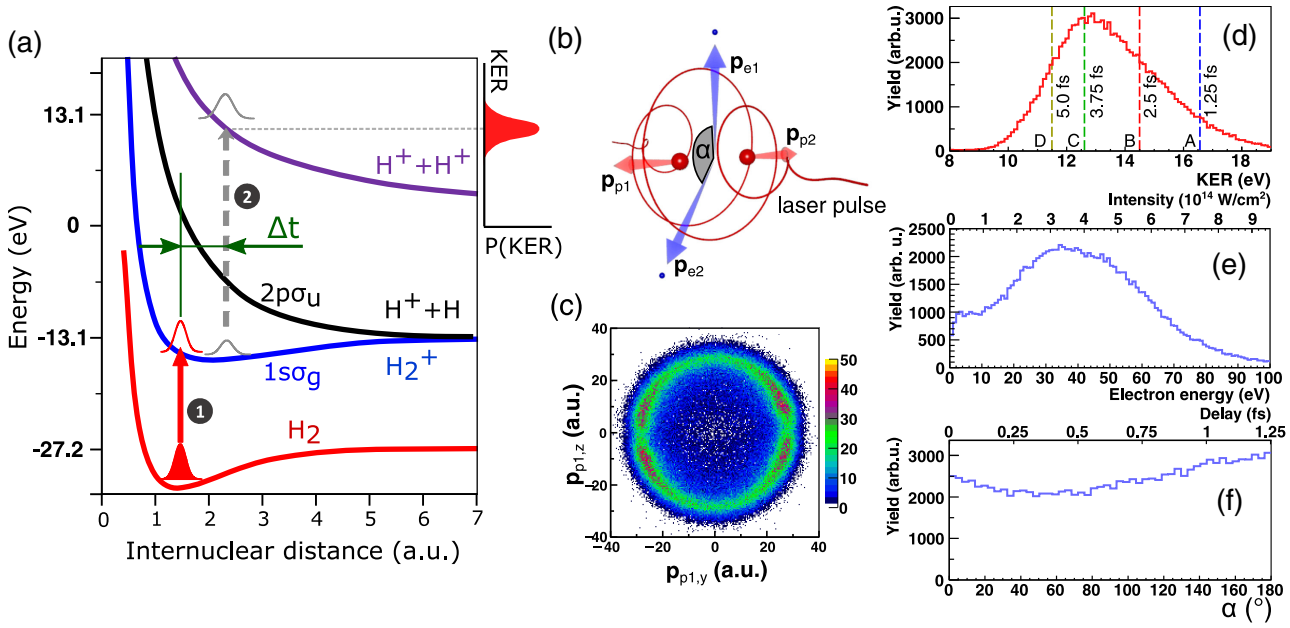

FIG. 1. (a) Schematics of the relevant potential energy surfaces of H_2. Indicated by arrows are the two ionization steps (❶ and ❷) delayed to each other by Δt. (b) Cartoon of the electron and ion momentum vectors after double ionization of H_2 in an intense elliptically polarized few-cycle laser pulse. (c) Distribution of the proton momentum from intrapulse double ionization in the polarization plane. The histogram is filled with two detected protons which satisfy a center-of-mass momentum < 10 a.u. The minimum around $p_{p1,z} = 0$ a.u. is due to the dead time of the detector. (d) Kinetic energy release. The lines A–D label certain values of Δt. (e) Photoelectron energy distribution. Upper axis: corresponding laser intensity. (f) Relative emission angle between the two photoelectrons. Upper axis: corresponding ionization delay on a subcycle scale.

vector $\mathbf{E}(t)$ completes a full rotation within one period of the field, $T = 2\pi/\omega$, where ω is the frequency of the light. This rotation serves as the minute hand of a clock: The ionization phase within a laser cycle ωt_i is mapped onto the emission angle of the photoelectron via the relation $\mathbf{p}_e = -\mathbf{A}(t_i)$, which is valid within the strong-field approximation [28,29], where the laser vector potential $\mathbf{A}(t)$ is connected to the laser electric field by $\mathbf{A}(t) = -\int_{-\infty}^{t} \mathbf{E}(t')dt'$. Thus, measurement of the electron emission angle in the laboratory frame determines the ionization time t_i within one cycle. In addition, the magnitude of the emitted electron's momentum vector $|\mathbf{p}_e|$ is proportional to the instantaneous field strength and thereby provides a measure about the ionization time within the pulse envelope [10].

The clock hand on the vibronic timescale is the kinetic energy release (KER) of the protons following double ionization. It has been shown that the KER, resulting from a Coulomb explosion of a molecule into two ionic fragments, is a sensitive measure of the distance R, where the repulsive Coulombic potential is populated [17,20,30–32]. In H_2, $\mathrm{KER} = (1/2m_p)(\mathbf{p}_{p1}^2 + \mathbf{p}_{p2}^2)$, with $\mathbf{p}_{p1,p2}$ the proton momenta and m_p their mass, the mapping $R = 1/\mathrm{KER}$ is very precise [18,33]. The first ionization event at time t_1 initiates a H_2^+ nuclear wave packet on the $1s\sigma_g$ ground state. The wave packet propagates on the light-induced potential energy surfaces and is projected onto the Coulombic potential energy curve by the second ionization event at time $t_2 = t_1 + \Delta t$, see Fig. 1(a). Measuring the momenta of the two protons provides us with the internuclear distance R at which the second ionization step happened. Hence, if the two ionization events are confined to within the first round-trip of the nuclear wave packet on the $1s\sigma_g$ potential we can establish a correlation between KER and Δt.

For the experiment we used reaction microscopy [34]. We measured the three-dimensional momentum vectors of two protons in coincidence with two electrons emerging from the interaction of H_2 molecules with elliptically polarized pulses with a broad spectrum centered around 750 nm (oscillation period $T = 2.5$ fs), a full width at half maximum (FWHM) duration in intensity of 4.5 fs, monitored by a phase-meter device [35], and a peak intensity of 9×10^{14} W cm^{-2}, calibrated *in situ* [36]. The experimental apparatus consists of a two-stage arrangement to provide an internally cold ultrasonic gas jet of hydrogen (along the y direction), and an interaction chamber with an ultrahigh vacuum (1.3×10^{-10} mbar). Electrons and ions were guided by weak magnetic (12 G) and electric (21 V/cm) fields along the spectrometer axis (z direction) to two position and time sensitive multihit detectors. The electron momentum resolution was 0.03, 0.80, and 0.45 a.u along the z, y, and x directions, respectively. Further details on the reaction microscope can be found in Refs. [3,37,38] and on the optical setup in Ref. [11] as well as in the Supplemental Material [39].

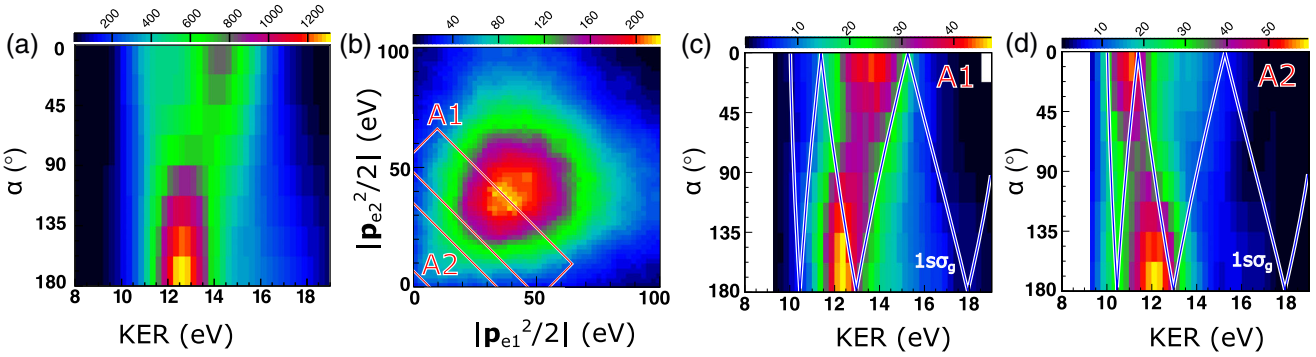

FIG. 2. (a) Double ionization yield as a function of kinetic energy release and the relative electron emission angle, integrated over the photoelectron energy. (b) Energy distribution of the two emitted photoelectrons (symmetrized about the diagonal). The marked areas $A1$, $A2$ correspond to regions of constant sum energy. Most of the photoelectrons are created with similar energies which indicates that the two-electron emission is symmetrically distributed around the laser pule peak. (c) Measured fragmentation yield as a function of α and KER obtained when the momenta of the two emitted electrons lie within range $A1$ indicated in (b). (d) Same as (c) but for electron momenta within range $A2$. The thin line in (c) and (d) shows the classical expectation value obtained for vibrational motion on the $1s\sigma_g$ potential energy curve (see text and Supplemental Material [39] for details).

Figure 1(c) shows the proton momentum distribution in the laser polarization plane for the double ionization pathway. The anisotropy of the proton distribution indicates the alignment of the polarization ellipse in the laboratory frame. In elliptical light, ionization preferentially takes place twice during the optical cycle [42]. Hence, sequential double ionization in elliptical light occurs with a delay between the two ionization steps of $\Delta t = nT/2$; $n = 0, 1, 2, \ldots$. To calibrate the zero of our timescale we turn to the KER, shown in Fig. 1(d). For instantaneous double ionization, i.e., $\Delta t = 0$, the H_2 ground state wave function would be projected vertically onto the Coulomb repulsion curve, to yield a KER distribution centered at 19 eV with a FWHM of 2 eV [33]. Thus, based on Fig. 1(d) we can exclude instantaneous double ionization in our experiment.

The observed KER distribution from 10 to 18 eV can be related to a timescale, assuming nuclear wave packet propagation on a given potential energy surface. To this end, we computed the nuclear-stretch motion in between the ionization times t_1 and $t_2 = t_1 + \Delta t$ by solving Newton's equations on the $1s\sigma_g$ energy curve [43]; see Supplemental Material [39] for details on the simulations. The simulation shows that our experiment covers a range of ionization delays starting from about $\Delta t = 0.5T$ (KER ≈ 18 eV) to roughly $\Delta t = 3T$ (KER ≈ 10 eV), with a maximum of the double ionization probability around $\Delta t = 1.5T$ (KER ≈ 13 eV). Smaller Δt values correspond to smaller internuclear distances, R, where the ionization potential is greatly increased and double ionization probability is accordingly suppressed, see Fig. 1(a). Double ionization delays of $\Delta t \lesssim 0.5T$ require both the increase of the pulse peak intensity and a pulse duration even shorter than the 4.5-fs pulses used here (Supplemental Material [39]).

The energy of each photoelectron, shown in Fig. 1(e), labels the light intensity at the instant of ionization. The peak at 40 eV corresponds to an ionization intensity of about 3.8×10^{14} W/cm^2. Therefore, the majority of double ionization events does not occur at the peak of the pulse, in agreement with the prediction of the double ionization delay based on the KER. Subcycle sensitivity, finally, is obtained from the relative angle $\alpha = \mathrm{ang}(\mathbf{p}_{e1}, \mathbf{p}_{e2})$ between the two photoelectron momenta $\mathbf{p}_{e1}$ and $\mathbf{p}_{e2}$, shown in Fig. 1(f). By virtue of the relation $\mathbf{p}_{e1,e2} = -\mathbf{A}(t_{1,2})$ the relative angle $\alpha \in [0°, 180°]$ directly measures Δt within one laser half-cycle. The minimum at $\alpha \approx 90°$ can be attributed to the ellipticity of the pulse. The relative emission angle peaks at $\alpha = 180°$, thus indicating a preferential double ionization at a delay of half-integer optical cycles, consistent with the $\Delta t = 1.5T$ deduced from the maximum of the KER distribution.

However, the estimates based on the isolated observables in Figs. 1(d)–1(f) do not yield a true subcycle resolution of the coupled electronic and nuclear dynamics. To obtain this, we will in the following examine the relation between KER, photoelectron emission angle, and energy to demonstrate how the subcycle dynamics of the nuclear wave packet can be accessed by correlating these three observables. In Fig. 2(a) we show the correlation between the two main hands of the molecular clock: the relative emission angle α of the photoelectrons and the KER of the protons. A previously indistinguishable maximum in the double ion yield at a KER of 14.5 eV is associated with a relative emission angle of zero degrees, i.e., the parallel emission of the two photoelectrons. The main maximum at a KER of 12.6 eV is slightly lower than in Fig. 1(d) and associated with antiparallel electron emission. Finally, a third peak at a KER of 11.5 eV and parallel emission is weakly distinguishable.

Thus, by correlating α with KER, we obtain a powerful parametric framework for representing the coupled electron and nuclear dynamics taking place in between the two

ionization steps. For example, if the $2p\sigma_u$ state is populated by shake-up during the first ionization step or also at later times by resonant transitions, the corresponding parametric curves in the α-KER frame of reference will look distinctively different from the one corresponding to vibrational motion on the $1s\sigma_g$ level; see Supplemental Material [39] for a comparison of curves obtained for different scenarios. Therefore, the ionization-fragmentation dynamics can be studied by comparison of the measured fragmentation yield to a simulated curve for a given scenario, e.g., for motion only on the $1s\sigma_g$ state.

Further insight into the molecular dynamics within the duration of the pulse can be obtained when the magnitudes of the photoelectron momenta $|\mathbf{p}_{e1,e2}|$ are analyzed. $|\mathbf{p}_{e1,e2}|$ provide an additional time reference linked to the fast rise time of a few-cycle pulse's envelope [10]. Gating on $|\mathbf{p}_{e1,e2}|$, thus allows selecting a range of ionization delays Δt. As a result, it becomes possible to obtain subcycle traces of the molecular dynamics for certain ranges of delays Δt in the two-electron emission and, moreover, as we will show further below, even attosecond snapshots of the propagating vibrational wave packet.

For the purpose of the following analysis we show the energies of both photoelectrons in Fig. 2(b). The highest double ionization probability is found for similar momenta of both electrons. Hence, the highest double ionization yield is from events where both electrons are emitted symmetrically around the peak of the pulse envelope. For example, the region $A1$ indicated in the correlated energy spectrum Fig. 2(b) corresponds to situations where both electrons are emitted within $\Delta t = 1.2T$–$1.7T$. Region $A2$ at smaller energies corresponds to emissions with longer delay, $\Delta t = 2.3T$–$3.2T$.

The capabilities opened up by the selection of the emission time-window based on $|\mathbf{p}^2_{e1,e2}/2|$ are demonstrated in Figs. 2(c) and 2(d). In these figures we show the measured distribution of the fragmentation yield in the α-KER plane for the two regions of electron energies $A1$ and $A2$ in Fig. 2(b). Accordingly, the corresponding ranges of the yield distribution in the α-KER plane in Figs. 2(c) and 2(d) show the vibrational wave packet evolution approximately in the time ranges of $1.2T$–$1.7T$ and $2.3T$–$3.2T$ after the first ionization step, respectively. A movie obtained for arbitrary selections of $|\mathbf{p}_{e1,e2}|$ is available as Supplemental Material [39]. The measured distributions in Figs. 2(c) and 2(d) are compared to the simulated curve obtained for wave packet motion on the $1s\sigma_g$ energy level (described in Supplemental Material [39]). The measured distributions show no signs of shake-up excitation that would appear for KER > 19 eV. Likewise, they show negligible yield in the range KER < 10 eV that corresponds to resonant excitation to the $2p\sigma_u$ energy curve. Laser field-induced distortions of the potential energy curves would also appear in this low KER range [44] and are thus not measured in our experiment. Overall,

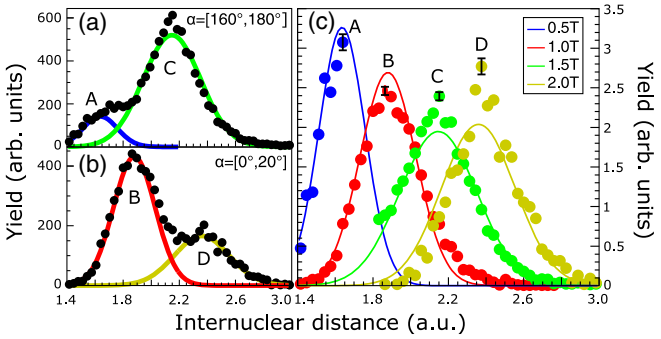

FIG. 3. Measured fragmentation yield (dots) over R for ionization events separated by an odd (a) and even (b) number of half cycles. (a) The distributions result from the selection $\alpha = [160°, 180°]$, corresponding to ionization events taking place within a range of ± 70 as around $\Delta t = (2n+1)(T/2)$, $n = 0, 1, 2$. (b) Same as (a) but for $\alpha = [0°, 20°]$, corresponding to ± 70 as around $\Delta t = 2n(T/2)$, $n = 0, 1, 2$. The colored lines labeled A–D are Gaussian fits to the data. The labels A–D correspond with those in Fig. 1. (c) Measured fragmentation yield (dots) from (a),(b) but with additional restrictions on the magnitude of the electron momentum (see Supplemental Material [39] for details), with statistical error bars, in comparison with the Gaussian fits from (a),(b). The areas of the distributions A–D were normalized to one.

the measured distributions agree well with the simulated curve for nuclear motion on the $1s\sigma_g$ curve, although there are some small deviations visible for the smaller emission delays Δt, cf. Fig. 2(c).

As $\alpha = 0$–$180°$ corresponds to one laser half cycle, by limiting α to small intervals, attosecond snapshots of the KER distribution can be extracted from these traces. By virtue of the Coulomb law, KER $= 1/R$ can be converted to internuclear distance R. Thus, it becomes possible to obtain snapshots of the absolute value of the vibrational wave packet, $|\chi(R, \Delta t)|^2$, for very short time intervals around certain values of Δt.

To obtain $|\chi|^2$ we select slices in the α-KER distribution for $\alpha = [0°, 20°]$ and $\alpha = [160°, 180°]$ corresponding to intervals of Δt of about 140 as. The yield distributions obtained by these selections are plotted in Figs. 3(a) and 3(b) as a function of R together with Gaussian fits. The Gaussian fits agree well with yield distributions obtained by more sophisticated selections (detailed in Supplemental Material [39]) that also involve gating on $|\mathbf{p}_{e1,e2}|$ as described above, see Fig. 3(c). The four distributions in Fig. 3(c) constitute snapshots of $|\chi(R, \Delta t)|^2$ with an uncertainty of about ± 70 as around $\Delta t = 0.5T, 1T, 1.5T, 2T$ and with a spatial resolution of about 0.02 a.u. (about 1 pm).

The equilibrium internuclear distance of H_2 is 1.4 a.u. Figure 3(c) shows that after half a laser cycle ($\Delta t = 1.25$ fs) the H_2^+ nuclear wave packet has propagated in distance by about 0.2 a.u. For larger values of Δt, our measurement reveals how the wave packet progressively moves to larger internuclear distances and spreads in space. Compared with

previous experiments that probed the nuclear motion of H_2^+ after strong-field laser ionization [18], our measurement is, to the best of our knowledge, the first one to reveal not only the position but also the shape of the wave packet. Additionally, our measurement probes the wave packet on a finer grid of Δt and with significantly higher temporal resolution (i.e., uncertainty in Δt).

In conclusion, we introduced a new method that allows tracing molecular dynamics on subfemtosecond times *during* strong-field interaction following field ionization. The method exploits the rotation of the electric field vector of elliptically polarized light as an attosecond temporal reference, and the dependence of the ion fragment energy on the molecular geometry as a clock for nuclear motion. Although demonstrated here for H_2, for which the nuclear clock shows a $1/R$ dependence, this is not a prerequisite of the method; any monotonic dependence of fragment energy on nuclear geometry is suitable. We therefore expect a wide applicability of the presented method and envision that it can also be applied to reasonably fast dissociative few-particle fragmentation channels in polyatomic molecules, as many of them fulfill this requirement. We highlight the high temporal resolution and spatial sensitivity of the method by demonstrating tracing of the vibrational wave packet evolution in H_2^+ with a temporal uncertainty of about ± 70 as and a spatial resolution of about 1 pm. The resolution of this technique can be expected to be further improved by exploitation of the carrier-envelope phase of few-cycle laser pulses [11].

This work was financed by the Austrian Science Fund (FWF), Grants No. P28475-N27 and No. P30465-N27.

*vaclav.hanus@tuwien.ac.at
†andre.staudte@nrc-cnrc.gc.ca
‡markus.kitzler@tuwien.ac.at

[1] M. F. Kling, P. von den Hoff, I. Znakovskaya, and R. de Vivie-Riedle, Phys. Chem. Chem. Phys. **15**, 9448 (2013).
[2] A. S. Alnaser and I. V. Litvinyuk, J. Phys. B **50**, 032002 (2017).
[3] X. Xie, K. Doblhoff-Dier, S. Roither, M. S. Schöffler, D. Kartashov, H. Xu, T. Rathje, G. G. Paulus, A. Baltuška, S. Gräfe, and M. Kitzler, Phys. Rev. Lett. **109**, 243001 (2012).
[4] X. Xie, S. Roither, M. Schöffler, E. Lötstedt, D. Kartashov, L. Zhang, G. G. Paulus, A. Iwasaki, A. Baltuška, K. Yamanouchi, and M. Kitzler, Phys. Rev. X **4**, 021005 (2014).
[5] X. Xie, E. Lötstedt, S. Roither, M. Schöffler, D. Kartashov, K. Midorikawa, A. Baltuška, K. Yamanouchi, and M. Kitzler, Sci. Rep. **5**, 12877 (2015).
[6] T. Ergler, A. Rudenko, B. Feuerstein, K. Zrost, C. D. Schröter, R. Moshammer, and J. Ullrich, Phys. Rev. Lett. **97**, 193001 (2006).
[7] H. Xu, F. He, D. Kielpinski, R. T. Sang, and I. V. Litvinyuk, Sci. Rep. **5**, 13527 (2015).
[8] C. Maharjan, A. Alnaser, X. Tong, B. Ulrich, P. Ranitovic, S. Ghimire, Z. Chang, I. Litvinyuk, and C. Cocke, Phys. Rev. A **72**, 041403(R) (2005).
[9] P. Eckle, M. Smolarski, P. Schlup, J. Biegert, A. Staudte, M. Schöffler, H. G. Muller, R. Dörner, and U. Keller, Nat. Phys. **4**, 565 (2008).
[10] A. N. Pfeiffer, C. Cirelli, M. Smolarski, R. Dörner, and U. Keller, Nat. Phys. **7**, 428 (2011).
[11] M. S. Schöffler, X. Xie, P. Wustelt, M. Möller, S. Roither, D. Kartashov, A. M. Sayler, A. Baltuska, G. G. Paulus, and M. Kitzler, Phys. Rev. A **93**, 063421 (2016).
[12] P. Wustelt, M. Möller, M. S. Schöffler, X. Xie, V. Hanus, A. M. Sayler, A. Baltuska, G. G. Paulus, and M. Kitzler, Phys. Rev. A **95**, 023411 (2017).
[13] J. Wu, M. Meckel, L. P. H. Schmidt, M. Kunitski, S. Voss, H. Sann, H. Kim, T. Jahnke, A. Czasch, and R. Dörner, Nat. Commun. **3**, 1113 (2012).
[14] J. Wu, L. P. H. Schmidt, M. Kunitski, M. Meckel, S. Voss, H. Sann, H. Kim, T. Jahnke, A. Czasch, and R. Dörner, Phys. Rev. Lett. **108**, 183001 (2012).
[15] J. Wu, M. Magrakvelidze, L. P. H. Schmidt, M. Kunitski, T. Pfeifer, M. Schöffler, M. Pitzer, M. Richter, S. Voss, H. Sann, H. Kim, J. Lower, T. Jahnke, A. Czasch, U. Thumm, and R. Dörner, Nat. Commun. **4**, 2177 (2013).
[16] X. Gong, Q. Song, Q. Ji, H. Pan, J. Ding, J. Wu, and H. Zeng, Phys. Rev. Lett. **112**, 243001 (2014).
[17] H. Stapelfeldt, E. Constant, H. Sakai, and P. B. Corkum, Phys. Rev. A **58**, 426 (1998).
[18] H. Niikura, F. Légaré, R. Hasbani, M. Y. Ivanov, D. M. Villeneuve, and P. B. Corkum, Nature (London) **421**, 826 (2003).
[19] F. Légaré, I. V. Litvinyuk, P. W. Dooley, F. Quéré, A. D. Bandrauk, D. M. Villeneuve, and P. M. Corkum, Phys. Rev. Lett. **91**, 093002 (2003).
[20] F. Légaré, K. F. Lee, I. V. Litvinyuk, P. W. Dooley, A. D. Bandrauk, D. M. Villeneuve, and P. B. Corkum, Phys. Rev. A **72**, 052717 (2005).
[21] S. Erattupuzha, C. L. Covington, A. Russakoff, E. Lötstedt, S. Larimian, V. Hanus, S. Bubin, M. Koch, S. Gräfe, A. Baltuška, X. Xie, K. Yamanouchi, K. Varga, and M. Kitzler, J. Phys. B **50**, 125601 (2017).
[22] A. Staudte, Ph. D. thesis, Johann Wolfgang Goethe Universität, Frankfurt am Main, 2005.
[23] H. Ibrahim, C. Lefebvre, A. D. Bandrauk, A. Staudte, and F. Légaré, J. Phys. B **51**, 042002 (2018).
[24] H. Niikura, F. Légaré, R. Hasbani, A. D. Bandrauk, M. Y. Ivanov, D. M. Villeneuve, and P. B. Corkum, Nature (London) **417**, 917 (2002).
[25] X. Urbain, B. Fabre, E. M. Staicu-Casagrande, N. de Ruette, V. M. Andrianarijaona, J. Jureta, J. H. Posthumus, A. Saenz, E. Baldit, and C. Cornaggia, Phys. Rev. Lett. **92**, 163004 (2004).
[26] I. V. Litvinyuk, F. Légaré, P. W. Dooley, D. M. Villeneuve, P. B. Corkum, J. Zanghellini, A. Pegarkov, C. Fabian, and T. Brabec, Phys. Rev. Lett. **94**, 033003 (2005).
[27] M. Haertelt, X.-B. Bian, M. Spanner, A. Staudte, and P. B. Corkum, Phys. Rev. Lett. **116**, 133001 (2016).
[28] F. Faisal, J. Phys. B **6**, L89 (1973).
[29] H. Reiss, Phys. Rev. A **22**, 1786 (1980).

[30] Z. Vager, R. Naaman, and E. P. Kanter, Science **244**, 426 (1989).
[31] S. Chelkowski, P. B. Corkum, and A. D. Bandrauk, Phys. Rev. Lett. **82**, 3416 (1999).
[32] H. Katsuki, H. Chiba, B. Girard, C. Meier, and K. Ohmori, Science **311**, 1589 (2006).
[33] T. Weber, A. O. Czasch, O. Jagutzki, A. K. Müller, V. Mergel, A. Kheifets, E. Rotenberg, G. Meigs, M. H. Prior, S. Daveau, A. Landers, C. L. Cocke, T. Osipov, R. Díez Muiño, H. Schmidt-Böcking, and R. Dörner, Nature (London) **431**, 437 (2004).
[34] R. Dörner, V. Mergel, O. Jagutzki, L. Spielberger, J. Ullrich, R. Moshammer, and H. Schmidt-Böcking, Phys. Rep. **330**, 95 (2000).
[35] A. M. Sayler, T. Rathje, W. Müller, C. Kürbis, K. Rühle, G. Stibenz, and G. G. Paulus, Opt. Express **19**, 4464 (2011).
[36] C. Smeenk, J. Z. Salvail, L. Arissian, P. B. Corkum, C. T. Hebeisen, and A. Staudte, Opt. Express **19**, 9336 (2011).
[37] L. Zhang, X. Xie, S. Roither, D. Kartashov, Y. L. Wang, C. L. Wang, M. Schöffler, D. Shafir, P. B. Corkum, A. Baltuška, I. Ivanov, A. Kheifets, X. J. Liu, A. Staudte, and M. Kitzler, Phys. Rev. A **90**, 061401 (2014).
[38] X. Xie, T. Wang, S. Yu, X. Lai, S. Roither, D. Kartashov, A. Baltuška, X. Liu, A. Staudte, and M. Kitzler, Phys. Rev. Lett. **119**, 243201 (2017).
[39] See Supplemental Material at http://link.aps.org/supplemental/10.1103/PhysRevLett.123.263201 for details of the experiment, data interpretation, and the numerical model, for which we made use of Refs. [40,41].
[40] X. M. Tong and C. D. Lin, Phys. Rev. A **70**, 023406 (2004).
[41] V. H. Dibeler, R. M. Reese, and M. Krauss, J. Chem. Phys. **42**, 2045 (1965).
[42] P. Eckle, A. N. Pfeiffer, C. Cirelli, A. Staudte, R. Dörner, H. G. Muller, M. Büttiker, and U. Keller, Science **322**, 1525 (2008).
[43] T. Sharp, At. Data Nucl. Data Tables **2**, 119 (1970).
[44] A. Giusti-Suzor, F. H. Mies, L. F. DiMauro, E. Charron, and B. Yang, J. Phys. B **28**, 309 (1995).